mathematics

MDPI

Article

A Dynamic Model of Cytosolic Calcium Concentration Oscillations in Mast Cells

Mingzhu Sun, Yingchen Li and Wei Yao *

Shanghai Key Laboratory of Acupuncture Mechanism and Acupoint Function, Department of Aeronautics and Astronautics, Fudan University, 220 Handan Road, Shanghai 200433, China; 19110290013@fudan.edu.cn (M.S.); 20110290014@fudan.edu.cn (Y.L.)

* Correspondence: weiyao@fudan.edu.cn

Abstract: In this paper, a dynamic model of cytosolic calcium concentration ($[Ca^{2+}]_{Cyt}$) oscillations is established for mast cells (MCs). This model includes the cytoplasm (Cyt), endoplasmic reticulum (ER), mitochondria (Mt), and functional region (μd), formed by the ER and Mt, also with Ca^{2+} channels in these cellular compartments. By this model, we calculate $[Ca^{2+}]_{Cyt}$ oscillations that are driven by distinct mechanisms at varying k_{deg} (degradation coefficient of inositol 1,4,5-trisphosphate, IP_3 and production coefficient of IP_3), as well as at different distances between the ER and Mt (ER–Mt distance). The model predicts that (i) Mt and μd compartments can reduce the amplitude of $[Ca^{2+}]_{Cyt}$ oscillations, and cause the ER to release less Ca^{2+} during oscillations; (ii) with increasing cytosolic IP_3 concentration ($[IP_3]_{Cyt}$), the amplitude of oscillations increases (from 0.1 μM to several μM), but the frequency decreases; (iii) the frequency of $[Ca^{2+}]_{Cyt}$ oscillations decreases as the ER–Mt distance increases. What is more, when the ER–Mt distance is greater than 65 nm, the μd compartment has less effect on $[Ca^{2+}]_{Cyt}$ oscillations. These results suggest that Mt, μd, and IP_3 can all affect the amplitude and frequency of $[Ca^{2+}]_{Cyt}$ oscillations, but the mechanism is different. The model provides a comprehensive mechanism for predicting cytosolic Ca^{2+} concentration oscillations in mast cells, and a theoretical basis for calcium oscillations observed in mast cells, so as to better understand the regulation mechanism of calcium signaling in mast cells.

Keywords: mathematical biology in general; mathematical modeling or simulation for problems pertaining to biology; mast cell; calcium oscillations; functional region formed by the ER and Mt; ER–Mt distance

check for updates

Citation: Sun, M.; Li, Y.; Yao, W. A Dynamic Model of Cytosolic Calcium Concentration Oscillations in Mast Cells. *Mathematics* **2021**, *9*, 2322. https://doi.org/10.3390/math9182322

Academic Editor: Mikhail Kolev

Received: 8 August 2021
Accepted: 15 September 2021
Published: 19 September 2021

1. Introduction

In recent years, more and more studies have found that mast cells (MCs) play a major role in the mechanism of acupuncture effect, and substances such as histamine and leukotriene, secreted by mast cells in the process of acupuncture, may be the key factors affecting acupuncture [1]. As an important second messenger, calcium signaling widely exists in various cell physiological processes, participating in the regulation of neurotransmitters released by neurons and astrocytes, metabolic processes, cell maturation, differentiation, and death [2–5]. The increase in cytosolic Ca^{2+} concentration ($[Ca^{2+}]_{Cyt}$) can be divided into the following two pathways: (i) the release of Ca^{2+} from the intracellular Ca^{2+} stores, mainly the endoplasmic reticulum (ER, the largest Ca^{2+} store), or (ii) extracellular Ca^{2+} influx to cytosol (Cyt), through the opening of plasma membrane Ca^{2+} channels. It has been widely accepted that Ca^{2+} release-activated Ca^{2+} (CARC) channels are the main mode of Ca^{2+} influx in electrically non-excitable cells, including MCs [6]. Meanwhile, it is also known that ER calcium depletion activates CRAC channels on the plasma membrane, leading to extracellular Ca^{2+} influx and endoplasmic reticulum Ca^{2+} supplementation. IP_3 interacts with Ca^{2+} channels in the ER, causing the release of stored Ca^{2+}, and the depletion of Ca^{2+} in the ER triggers Ca^{2+} entry through CRAC channels. CRAC channels in MCs are

non-voltage-gated and show a characteristic inward rectification [7]. Therefore, the Ca^{2+} flow of CRAC channels is related to the Ca^{2+} concentration of the ER and Cyt. In contrast to the CRAC channels, the plasma membrane Ca^{2+}-ATPase (PMCA) channels extrude Ca^{2+} to the extracellular space, to maintain calcium concentration balance. They can transfer Ca^{2+} against the concentration gradient in the presence of ATP [8]. Previously, we believed that the mitochondria (Mt, the second largest calcium store) only play a role in regulating cytosolic calcium concentration under the pathological condition of very high intracellular calcium ion concentration [9]. Until the 1990s, there were studies demonstrating that the non-pathological increase of cytosolic calcium concentration was accompanied by Ca^{2+} concentration increasing in the mitochondrial matrix ($[Ca^{2+}]_{Mt}$) [10]. Moreover, recent studies have shown that the Mt regulate Ca^{2+} oscillations by firstly uptaking Ca^{2+}, and subsequently releasing it [11–14]. The evidence was supported by the discovery of the functional region formed by the ER and Mt (μd) [15–17]. The functional region is composed of the Mt membrane, ER membrane, and Cyt between them. However, the assumption distances of μd vary hugely, from less than 10 nm to more than 200 nm [18]. When mast cells are mechanically stimulated, the intracellular Ca^{2+} concentration will increase, then leukotriene C_4 (LTC_4) will be produced, which can activate phospholipase C (PLC), to promote PIP_2 decomposition to IP_3 [19]. Subsequently, IP_3 binds to the inositol 1,4,5-trisphosphate receptor (IP_3R) on the ER membrane, which induces Ca^{2+} release from the ER. IP_3R is regulated by Ca^{2+} in a biphasic manner (stimulatory at low levels/inhibitory at high levels) [19–22]. The mitochondrial Ca^{2+} uniporter (MCU) in mitochondria uptakes Ca^{2+} quickly when exposed to high Ca^{2+} concentration environments around the opened IP_3R channel pore. MCs are activated by mechanical stimulation, and the Ca^{2+} concentration in μd can reach more than 10 times that in the cytoplasm, which was enough to activate the mitochondrial MCU channel and allow Ca^{2+} uptake [23–25]. This explains why high Ca^{2+} is observed when global Ca^{2+} is low.

In order to better explore the physiological mechanism of calcium oscillations, researchers have carried out a large number of experiments. For example, Joseph Di Capite et al. [26] recorded calcium waves in mast cells, and studied the effects of CARC channels on them. Osipchuk et al. [27] studied the effect of ATP on calcium signaling spread between mast cells, and recorded the calcium signaling. At the same time, mathematical modeling can establish the internal relationship between experimental data and parameters, and predict the possible phenomena, so as to save time and cost. In the early years, Goldbeter et al. [28], Hofer [29], and Li and Rinzel [30] described calcium oscillations that only consider the function of the endoplasmic reticulum, while little consider the influences of the mitochondria. Based on the Ca^{2+} dynamic model proposed by Othmer-Tang et al., Falcke et al. [31] added the mitochondrial Ca^{2+} cycle equation into the model. Shi [32] and Qi et al. [33] established a theoretical model, considering the influences of the mitochondria. They explored the effect of the interaction between the mitochondria and the endoplasmic reticulum on calcium oscillations. Arash Moshkforoush et al. [34] developed a compartmental closed-cell mathematical model of Ca^{2+} dynamics that includes a functional region between the ER and Mt. However, they do not consider the effect of plasma membrane calcium channels and the extracellular Ca^{2+} concentration on intracellular calcium oscillations. Although there are many mathematical models that describe calcium oscillations, most of them only consider the effects of the endoplasmic reticulum. Therefore, in order to explain the calcium signaling observed in mast cells, and explore the influence of each compartment on oscillations more accurately, a comprehensive dynamic model of $[Ca^{2+}]_{Cyt}$ oscillations is established in this paper. This model takes the following cellular compartments into account: plasma membrane (Mem), cytoplasm (Cyt), endoplasmic reticulum (ER), and mitochondria (Mt). The major Ca^{2+} channels and Ca^{2+} buffering in these compartments are considered. The functional region formed by the ER and Mt (μd) is explicitly assumed as a Ca^{2+} pool. The degradation and production of IP_3 is added to this model, to investigate the effect of IP_3 dynamics on $[Ca^{2+}]_{Cyt}$ oscillations.

2. Mathematical Model

The full model includes plasma membrane channels, and degradation and production of IP_3, Cyt, ER, Mt, and μd. MCs will release IP_3 after they are activated by mechanical stimuli. Then, IP_3 bines to IP_3R to trigger the intracellular Ca^{2+} signal. The whole progress is shown in Figure 1. Calcium dynamics in each compartment are governed by a balance of Ca^{2+} fluxes, leaks, and buffering processes.

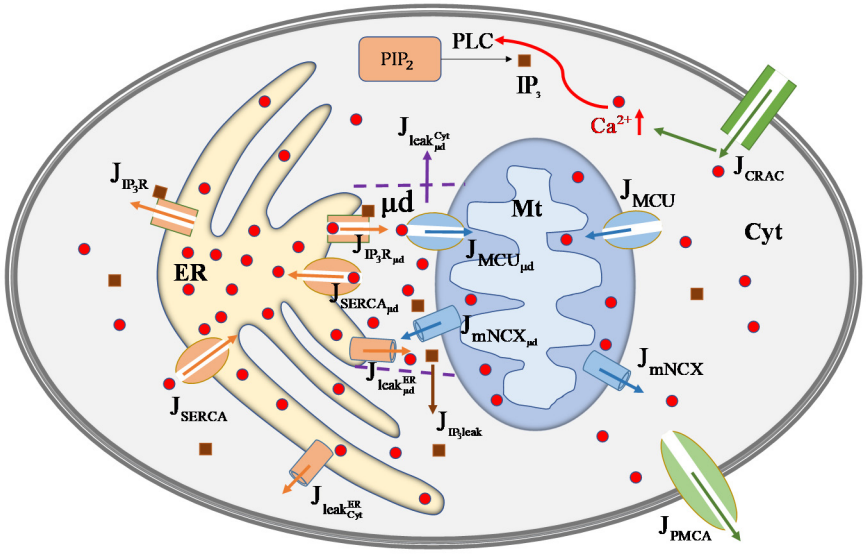

Figure 1. Schematic diagram of the regulation mechanism of cellular calcium concentration. After stimulation, Ca^{2+} enters the mast cell through the Ca^{2+} release-activated Ca^{2+} (CARC) channels on Mem and increases $[Ca^{2+}]_{Cyt}$. Then PIP_2 is catalyzed by PLC to produce IP_3. IP_3 binds to IP_3R to activate Ca^{2+} releases from ER. Endoplasmic reticulum Ca^{2+}-ATPase (SERCA) pump uptakes Ca^{2+} to ER. Ca^{2+} leaks from ER by leak channel. Mt uptakes Ca^{2+} through the MCU channel and extrudes Ca^{2+} via the mitochondrial Na^+/Ca^{2+} exchanger (mNCX). These Ca^{2+} channels in ER and Mt can face either Cyt or μd. Ca^{2+} and IP_3 can diffuse between Cyt and μd. Ca^{2+} is extruded from Cyt to extracellular matrix through the plasma membrane Ca^{2+}-ATPase (PMCA) channels. J means calcium fluxes, such as J_{IP_3R} means the Ca^{2+} outflux of IP_3R channels.

2.1. Cross-Membrane Ca^{2+} Current

According to previous researches, we accept that CRAC channels and plasma membrane Ca^{2+}-ATPase (PMCA) channels are the main Ca^{2+} channels in MCs [33]. CRAC channels are Ca^{2+} influx channels, and PMCA channels are Ca^{2+} outflux channels. The CRAC current is given by the Hodgkin–Huxley (HH) model [35], as follows:

$$I_{\mathrm{CRAC}} = g_{\mathrm{CRAC}} \cdot P_{\mathrm{CRAC}} \cdot (E_{\mathrm{m}} - E_{\mathrm{Ca}}) \tag{1}$$

where g_{CRAC} is the conductance, E_{m} is the membrane potential, and $E_{\mathrm{Ca}} = \phi \cdot \log \frac{[\mathrm{Ca}^{2+}]_{\mathrm{e}}}{[\mathrm{Ca}^{2+}]_{\mathrm{Cyt}}}$ is the Nernst potential for Ca^{2+}, $\phi = \frac{RT}{zF}$, where R is the universal gas constant, T is the absolute temperature, $z = 2$ is the valence of Ca^{2+}, and F is the Faraday constant. P_{CRAC} is the proportion of CRAC channels in open state, and it is assumed as follows [35]:

$$P_{\mathrm{CRAC}} = \frac{[\mathrm{Ca}^{2+}]_{\mathrm{act}\frac{1}{2}}}{[\mathrm{Ca}^{2+}]_{\mathrm{act}\frac{1}{2}} + [\mathrm{Ca}^{2+}]_{\mathrm{ER}}} \tag{2}$$

The PMCA current is given by the following [36]:

$$I_{\mathrm{PMCA}} = I_{\mathrm{PMCA,M}} \cdot \frac{[\mathrm{Ca}^{2+}]_{\mathrm{Cyt}}}{K_{\mathrm{PMCA}} + [\mathrm{Ca}^{2+}]_{\mathrm{Cyt}}} \tag{3}$$

where $I_{\mathrm{PMCA,M}}$ is the maximum PMCA current, and K_{PMCA} is the Ca^{2+} concentration for the half activation of PMCA channels.

2.2. Ca^{2+} Outflows from ER

The calcium outflow from the ER to Cyt or μd, through $\mathrm{IP_3R}$ channels, is defined as follows:

$$J_{\mathrm{IP3R}} = (1 - C_{\mathrm{IP3R}}) \cdot (V_{\mathrm{IP3R}} P_{\mathrm{oIP3R}}) \cdot ([\mathrm{Ca}^{2+}]_{\mathrm{ER}} - [\mathrm{Ca}^{2+}]_{\mathrm{Cyt}}) \tag{4}$$

$$J_{\mathrm{IP3R}_{\mu\mathrm{d}}} = C_{\mathrm{IP3R}} \cdot (V_{\mathrm{IP3R}} P_{\mathrm{oIP3R}_{\mu\mathrm{d}}}) \cdot ([\mathrm{Ca}^{2+}]_{\mathrm{ER}} - [\mathrm{Ca}^{2+}]_{\mu\mathrm{d}}) \tag{5}$$

where V_{IP3R} is the maximum total flux through $\mathrm{IP_3R}$ channels [33], and P_{oIP3R} and $P_{\mathrm{oIP3R}_{\mu\mathrm{d}}}$ are the open probabilities of $\mathrm{IP_3R}$ channels facing the Cyt and μd, respectively, and they are defined as follows [33]:

$$P_{\mathrm{oIP3R}} = S_{\mathrm{act}}^4 + 4S_{\mathrm{act}}^3 \cdot (1 - S_{\mathrm{act}}) \tag{6}$$

$$S_{\mathrm{act}} = \left(\frac{[\mathrm{IP}_3]_{\mathrm{Cyt}}}{[\mathrm{IP}_3]_{\mathrm{Cyt}} + d_1}\right) \cdot \left(\frac{[\mathrm{Ca}^{2+}]_{\mathrm{Cyt}}}{[\mathrm{Ca}^{2+}]_{\mathrm{Cyt}} + d_5}\right) \cdot h \tag{7}$$

$$P_{\mathrm{oIP3R}_{\mu\mathrm{d}}} = S_{\mathrm{act}_{\mu\mathrm{d}}}^4 + 4S_{\mathrm{act}_{\mu\mathrm{d}}}^3 \cdot (1 - S_{\mathrm{act}_{\mu\mathrm{d}}}) \tag{8}$$

$$S_{\mathrm{act}_{\mu\mathrm{d}}} = \left(\frac{[\mathrm{IP}_3]_{\mu\mathrm{d}}}{[\mathrm{IP}_3]_{\mu\mathrm{d}} + d_1}\right) \cdot \left(\frac{[\mathrm{Ca}^{2+}]_{\mu\mathrm{d}}}{[\mathrm{Ca}^{2+}]_{\mu\mathrm{d}} + d_5}\right) \cdot h_{\mu\mathrm{d}} \tag{9}$$

where S_{act} and $S_{\mathrm{act}_{\mu\mathrm{d}}}$ express the probability of the activated subunit, respectively, and are defined by sigmoidal functions of $[\mathrm{IP}_3]$ and $[\mathrm{Ca}^{2+}]_{\mathrm{Cyt}}$, and h is the slow inactivation gating variable, defined as follows:

$$\frac{dh}{dt} = \alpha_{\mathrm{h}}(1 - h) - \beta_{\mathrm{h}} h \tag{10}$$

$$\alpha_{\mathrm{h}} = a_2 d_2 \cdot \left(\frac{[\mathrm{IP}_3]_{\mathrm{Cyt}} + d_1}{[\mathrm{IP}_3]_{\mathrm{Cyt}} + d_3}\right) \tag{11}$$

$$\beta_{\mathrm{h}} = a_2 \cdot [\mathrm{Ca}^{2+}]_{\mathrm{Cyt}} \tag{12}$$

for μd, it is the following:

$$\frac{dh_{\mu\mathrm{d}}}{dt} = \alpha_{\mathrm{h}}(1 - h_{\mu\mathrm{d}}) - \beta_{\mathrm{h}_{\mu\mathrm{d}}} h_{\mu\mathrm{d}} \tag{13}$$

$$\beta_{\mathrm{h}_{\mu\mathrm{d}}} = a_2 \cdot [\mathrm{Ca}^{2+}]_{\mu\mathrm{d}} \tag{14}$$

where a_2, d_1, d_2, d_3, and d_5 are parameters.

For $\mathrm{IP_3}$ dynamics, the production speed of $\mathrm{IP_3}$ is related to PLC, and the production of phospholipase C isoforms depends on $[\mathrm{Ca}^{2+}]_{\mathrm{Cyt}}$, so the production speed of $\mathrm{IP_3}$ is defined as follows:

$$J_{\mathrm{IP_3pro}_{\mathrm{Cyt}}} = V_{\mathrm{PLC}} \frac{[\mathrm{Ca}^{2+}]_{\mathrm{Cyt}}^2}{K_{\mathrm{PLC}}^2 + [\mathrm{Ca}^{2+}]_{\mathrm{Cyt}}^2} \tag{15}$$

for μd, it is as follows:

$$J_{\mathrm{IP_3pro_{\mu d}}} = V_{\mathrm{PLC}} \frac{[\mathrm{Ca}^{2+}]^2_{\mu d}}{K^2_{\mathrm{PLC}} + [\mathrm{Ca}^{2+}]^2_{\mu d}} \tag{16}$$

where V_{PLC} is the maximal production rate of PLC isoforms, and K_{PLC} is the sensitivity of PLC to Ca^{2+}.

IP_3 is degraded through phosphorylation by IP_3 kinases. The kinetic equation can be written as follows:

$$J_{\mathrm{IP_3deg_{Cyt}}} = k_{\mathrm{deg}} \frac{[\mathrm{Ca}^{2+}]^2_{\mathrm{Cyt}}}{K^2_{\mathrm{deg}} + [\mathrm{Ca}^{2+}]^2_{\mathrm{Cyt}}} [\mathrm{IP}_3]_{\mathrm{Cyt}} \tag{17}$$

for μd, it as follows:

$$J_{\mathrm{IP_3deg_{\mu d}}} = k_{\mathrm{deg}} \frac{[\mathrm{Ca}^{2+}]^2_{\mu d}}{K^2_{\mathrm{deg}} + [\mathrm{Ca}^{2+}]^2_{\mu d}} [\mathrm{IP}_3]_{\mu d} \tag{18}$$

where k_{deg} represents the phosphorylation rate constants, and K_{deg} is the half-saturation constant of IP_3 kinases.

IP_3 leaks from μd to Cyt can be defined as follows:

$$J_{\mathrm{IP_3leak}} = k_{\mathrm{IP_3leak}}([\mathrm{IP}_3]_{\mu d} - [\mathrm{IP}_3]_{\mathrm{Cyt}}). \tag{19}$$

Therefore, the change in $[\mathrm{IP}_3]_{\mathrm{Cyt}}$ and $[\mathrm{IP}_3]_{\mu d}$ can be written as follows:

$$\frac{d[\mathrm{IP}_3]_{\mathrm{Cyt}}}{dt} = J_{\mathrm{IP_3pro_{Cyt}}} - J_{\mathrm{IP_3deg_{Cyt}}} + J_{\mathrm{IP_3leak}} \tag{20}$$

$$\frac{d[\mathrm{IP}_3]_{\mu d}}{dt} = J_{\mathrm{IP_3pro_{\mu d}}} - J_{\mathrm{IP_3deg_{\mu d}}} - J_{\mathrm{IP_3leak}} \tag{21}$$

SERCA pumps transport Ca^{2+} into the ER, and the flux from Cyt to the ER is defined as follows:

$$J_{\mathrm{SERCA}} = (1 - C_{\mathrm{SERCA}}) \cdot V_{\mathrm{SERCA}} \cdot \left(\frac{[\mathrm{Ca}^{2+}]^2_{\mathrm{Cyt}}}{k^2_{\mathrm{SERCA}} + [\mathrm{Ca}^{2+}]^2_{\mathrm{Cyt}}}\right) \tag{22}$$

the flux from μd to the ER is defined as follows:

$$J_{\mathrm{SERCA_{\mu d}}} = C_{\mathrm{SERCA}} \cdot V_{\mathrm{SERCA}} \cdot \left(\frac{[\mathrm{Ca}^{2+}]^2_{\mu d}}{k^2_{\mathrm{SERCA}} + [\mathrm{Ca}^{2+}]^2_{\mu d}}\right) \tag{23}$$

where V_{SERCA} is the maximal flux through SERCA, and k_{SERCA} is the Ca^{2+} activation constant for SERCA.

Ca^{2+} leaks from the the ER are driven by the concentration gradients between the ER and either the Cyt or μd. The leak from the ER into the Cyt is defined as follows:

$$J_{\mathrm{leak^{ER}_{Cyt}}} = k^{\mathrm{ER}}_{\mathrm{Cyt}} \cdot ([\mathrm{Ca}^{2+}]_{\mathrm{ER}} - [\mathrm{Ca}^{2+}]_{\mathrm{Cyt}}) \tag{24}$$

and the leak from the ER into the μd is defined as follows:

$$J_{\mathrm{leak^{ER}_{\mu d}}} = k^{\mathrm{ER}}_{\mu d} \cdot ([\mathrm{Ca}^{2+}]_{\mathrm{ER}} - [\mathrm{Ca}^{2+}]_{\mu d}) \tag{25}$$

Although the μd is not a membrane-bound compartment, we similarly define the leak from the μd into the Cyt as follows:

$$J_{\mathrm{leak^{\mu d}_{Cyt}}} = k^{\mu d}_{\mathrm{Cyt}} \cdot ([\mathrm{Ca}^{2+}]_{\mu d} - [\mathrm{Ca}^{2+}]_{\mathrm{Cyt}}) \tag{26}$$

2.3. Ca^{2+} Outflows from Mt

In the Mt, the mNCX channels exchange one Ca^{2+} for three Na^{+}. Flux through mNCX channels facing the Cyt is defined as follows:

$$J_{\mathrm{mNCX}} = (1 - C_{\mathrm{mNCX}}) \cdot V_{\mathrm{mNCX}} \cdot \left(\frac{[\mathrm{Na}^{+}]^{3}_{\mathrm{Cyt}}}{k^{3}_{\mathrm{Na}} + [\mathrm{Na}^{+}]^{3}_{\mathrm{Cyt}}}\right) \cdot \left(\frac{[\mathrm{Ca}^{2+}]_{\mathrm{Mt}}}{k_{\mathrm{mNCX}} + [\mathrm{Ca}^{2+}]_{\mathrm{Mt}}}\right) \tag{27}$$

and for mNCX channels facing the μd, it is as follows:

$$J_{\mathrm{mNCX}_{\mu\mathrm{d}}} = C_{\mathrm{mNCX}} \cdot V_{\mathrm{mNCX}} \cdot \left(\frac{[\mathrm{Na}^{+}]^{3}_{\mu\mathrm{d}}}{k^{3}_{\mathrm{Na}} + [\mathrm{Na}^{+}]^{3}_{\mu\mathrm{d}}}\right) \cdot \left(\frac{[\mathrm{Ca}^{2+}]_{\mathrm{Mt}}}{k_{\mathrm{mNCX}} + [\mathrm{Ca}^{2+}]_{\mathrm{Mt}}}\right) \tag{28}$$

where $[\mathrm{Na}^{+}]_{\mathrm{Cyt}}$ and $[\mathrm{Na}^{+}]_{\mu\mathrm{d}}$ are the concentration of Na^{+} in Cyt and μd, respectively. V_{mNCX} is the maximal flux through the mNCX, and k_{Na} and k_{mNCX} are Na^{+} and Ca^{2+} activation constants for mNCX, respectively. The connectivity coefficient C_{mNCX} is the proportion of mNCX channels facing the μd.

The MCU channel transports Ca^{2+} into the Mt. Flux through the MCU to the Cyt is defined as follows:

$$J_{\mathrm{MCU}} = (1 - C_{\mathrm{MCU}}) \cdot V_{\mathrm{MCU}} \cdot \left(\frac{[\mathrm{Ca}^{2+}]^{2}_{\mathrm{Cyt}}}{k^{2}_{\mathrm{MCU}} + [\mathrm{Ca}^{2+}]^{2}_{\mathrm{Cyt}}}\right) \tag{29}$$

and to the μd, it is as follows:

$$J_{\mathrm{MCU}_{\mu\mathrm{d}}} = C_{\mathrm{MCU}} \cdot V_{\mathrm{MCU}} \cdot \left(\frac{[\mathrm{Ca}^{2+}]^{2}_{\mu\mathrm{d}}}{k^{2}_{\mathrm{MCU}} + [\mathrm{Ca}^{2+}]^{2}_{\mu\mathrm{d}}}\right) \tag{30}$$

where $V_{\mathrm{MCU}} = V_{\mathrm{MCU}_0}\Delta\Phi$, and $\Delta\Phi = \frac{bF(\Psi - \Psi_0)}{RT} e^{\frac{bF(\Psi - \Psi_0)}{RT}} \sinh \frac{bF(\Psi - \Psi_0)}{RT}$. V_{MCU_0} represents the maximal flux through the MCU, and $\Delta\Phi$ is the voltage driving force. Ψ is the inner mitochondrial membrane voltage (150~180 mV, negative inside). b and Ψ_0 are the fitting parameters obtained from Qi [33]. During the simulations, we assume a constant Ψ of 170 mV, as experimental evidence suggests that Ψ does not change significantly in response to transient cytosolic $[\mathrm{Ca}^{2+}]$ increase, produced by IP_3-generating agonists [37–39]. k_{MCU} is the Ca^{2+} activation constant for MCU, and the connectivity coefficient C_{MCU} is the proportion of MCU channels facing the μd.

2.4. Effective Cytosol

Since the μd is a part of the cytosol, we defined the $[\mathrm{Ca}^{2+}]$ of the effective cytosolic compartment $[\mathrm{Ca}^{2+}]^{\mathrm{eff}}_{\mathrm{Cyt}}$ as the volume-weighted average of $[\mathrm{Ca}^{2+}]$ within the combined Cyt and μd compartments.

$$[\mathrm{Ca}^{2+}]^{\mathrm{eff}}_{\mathrm{Cyt}} = \frac{Vol_{\mathrm{Cyt}} \cdot [\mathrm{Ca}^{2+}]_{\mathrm{Cyt}} + Vol_{\mu\mathrm{d}} \cdot [\mathrm{Ca}^{2+}]_{\mu\mathrm{d}}}{Vol_{\mathrm{Cyt}} + Vol_{\mu\mathrm{d}}} \tag{31}$$

2.5. μd Volume

We assumed that each mitochondrion is a sphere, and 20% of its surface area closes to the ER [18,40]. Some experimental data suggest that the diameters of mitochondria are 0.5~1.5 μm [41]; here, we choose 0.58 μm. There are about two hundred (N) mitochondria in each cell. Thus, we calculate the volume of the μd compartment as follows:

$$Vol_{\mu\mathrm{d}} = 0.2 \cdot SA \cdot N \cdot D \tag{32}$$

where SA is the surface area, N is the mitochondria total number, and D is the ER–Mt distance.

2.6. Temporal Changes in $[Ca^{2+}]$ in Each Compartment

Temporal changes in $[\mathrm{Ca}^{2+}]$ in each compartment are represented as the following ordinary differential equations:

in cytosol, it is the following:

$$\frac{d[\mathrm{Ca}^{2+}]_{\mathrm{Cyt}}}{dt} = \frac{(J_{\mathrm{IP3R}} + J_{\mathrm{mNCX}} + J_{\mathrm{leak}^{\mu d}_{\mathrm{Cyt}}} + J_{\mathrm{leak}^{\mathrm{ER}}_{\mathrm{Cyt}}} - J_{\mathrm{SERCA}} - J_{\mathrm{MCU}})}{1 + \theta_{\mathrm{Cyt}}} + \frac{S_c}{zFVol_{\mathrm{Cyt}}}(I_{\mathrm{CRAC}} - I_{\mathrm{PMCA}}) \tag{33}$$

in the ER, it is the following:

$$\frac{d[\mathrm{Ca}^{2+}]_{\mathrm{ER}}}{dt} = \frac{Vol_{\mathrm{Cyt}}}{Vol_{\mathrm{ER}}}\,(J_{\mathrm{SERCA}} + J_{\mathrm{SERCA}_{\mu d}} - J_{\mathrm{IP3R}} - J_{\mathrm{IP3R}_{\mu d}} - J_{\mathrm{leak}^{\mathrm{ER}}_{\mu d}} - J_{\mathrm{leak}^{\mathrm{ER}}_{\mathrm{Cyt}}})/(1 + \theta_{\mathrm{ER}}) \tag{34}$$

in the Mt, it is the following:

$$\frac{d[\mathrm{Ca}^{2+}]_{\mathrm{Mt}}}{dt} = \frac{Vol_{\mathrm{Cyt}}}{Vol_{\mathrm{Mt}}}\,(J_{\mathrm{MCU}} + J_{\mathrm{MCU}_{\mu d}} - J_{\mathrm{mNCX}} - J_{\mathrm{mNCX}_{\mu d}})/(1 + \theta_{\mathrm{Mt}}) \tag{35}$$

in μd, it is the following:

$$\frac{d[\mathrm{Ca}^{2+}]_{\mu d}}{dt} = \frac{Vol_{\mathrm{Cyt}}}{Vol_{\mu d}}(J_{\mathrm{IP3R}_{\mu d}} + J_{\mathrm{mNCX}_{\mu d}} + J_{\mathrm{leak}^{\mathrm{ER}}_{\mu d}} - J_{\mathrm{SERCA}_{\mu d}} - J_{\mathrm{MCU}_{\mu d}} - J_{\mathrm{leak}^{\mu d}_{\mathrm{Cyt}}})/(1 + \theta_{\mu d}) \tag{36}$$

where θ_{i} (i = Cyt, ER, Mt, μd) is the buffer factor of each compartment, which is defined as follows [36]:

$$\theta_{\mathrm{i}} = \frac{BP_{\mathrm{i}}K_{\mathrm{i}}}{([\mathrm{Ca}^{2+}]_{\mathrm{i}} + K_{\mathrm{i}})^2} \tag{37}$$

The parameter values related to our model are given in Table 1.

Table 1. Parameters of the model.

Parameter	Value	Description
g_{CRAC}	$0.3\ \Omega^{-1}\ \mathrm{m}^{-2}$	the conductance [19]
E_{m}	-60 mV	the membrane potential [19]
R	$8.34\ \mathrm{J\ mol^{-1}\ K^{-1}}$	the universal gas constant [19]
T	293 K	the absolute temperature [19]
F	$96,485\ \mathrm{C\ mol^{-1}}$	Faraday constant [19]
$[\mathrm{Ca}^{2+}]_{\mathrm{act1/2}}$	$5 \times 10^{-4}\ \mathrm{mol\ L^{-1}}$	the Ca^{2+} concentration for half activation of SOC [19]
$I_{\mathrm{PMCA,M}}$	$89.9\ \mu\mathrm{M\ s^{-1}}$	the maximum PMCA current [36]
K_{PMCA}	0.26 μM	the Ca^{2+} concentration for half activation of PMCA channels [36]
$[\mathrm{Ca}^{2+}]_{\mathrm{e}}$	2000 μM	the extracellular Ca^{2+} concentration [19]
Vol_{ER}	0.1 pL	volume of ER [41]
Vol_{Mt}	0.05 pL	volume of Mt [41]
Vol_{Cyt}	0.85 pL	volume of Cyt [34]
S_c	$0.28\ \mathrm{pm}^2$	cell surface [34]
V_{IP3R}	$1.59\ \mathrm{s^{-1}}$	max flux of IP_3R [34]
V_{SERCA}	$29.1\ \mu\mathrm{M\ s^{-1}}$	max flux of SERCA pump [34]
k_{SERCA}	0.193 μM	activation constant for SERCA pump [34]
a_2	$0.0605\ \mu\mathrm{M^{-1}\ s^{-1}}$	IP_3R binding rate at Ca^{2+} inhibition sites [34]
d_1	0.0377 μM	IP_3R dissociation constant for IP_3 sites [34]
d_2	1.33 μM	IP_3R dissociation constant for Ca^{2+} inhibition sites [34]
d_3	1.74 μM	IP_3R dissociation constant for IP_3 sites [34]
d_5	0.239 μM	IP_3R dissociation constant for Ca^{2+} activation sites [34]
V_{MCU}	$7.53\ \mu\mathrm{M\ s^{-1}}$	max rate of Ca^{2+} uptake by MCU [34]
k_{MCU}	1.23 μM	half-max rate of Ca^{2+} pumping from Cyt to Mt [34]
V_{NCX}	$119\ \mu\mathrm{M\ s^{-1}}$	max rate of Ca^{2+} release through NCX [34]

Table 1. *Cont.*

Parameter	Value	Description
k_{NCX}	43.2 μM	activation constant for NCX [34]
k_{Na}	9.4 mM	Na^+ activation constant for MCU [34]
$[Na]_{Cyt}$	10 mM	Na^+ in Cyt [34]
$[Na]_{\mu d}$	10 mM	Na^+ in μd [34]
$k_{\mu d}^{ER}$	0.0433 s^{-1}	leak constant from ER to μd [34]
k_{Cyt}^{ER}	0.0107 s^{-1}	leak constant from ER to Cyt [34]
$k_{Cyt}^{\mu d}$	0.0332 s^{-1}	leak constant from μd to Cyt [34]
C_{IP3R}	0.486	fraction of IP_3R facing microdomain [34]
C_{SERCA}	0.603	fraction of SERCA facing microdomain [34]
C_{MCU}	0.894	fraction of MCU facing microdomain [34]
C_{mNCX}	0.569	fraction of mNCX facing microdomain [34]
BP_{Cyt}	154 μM	total buffer concentration in Cyt [42]
K_{Cyt}	11.1	buffer rate constant ratio [42]
BP_{ER}	11,100 μM	total buffer concentration in ER [42]
K_{ER}	967	buffer rate constant ratio [42]
BP_{Mt}	285,000 μM	total buffer concentration in Mt [42]
K_{Mt}	698	buffer rate constant ratio [42]
$BP_{\mu d}$	191 μM	total buffer concentration in μd [42]
$K_{\mu d}$	12	buffer rate constant ratio [42]

3. Results

3.1. Effect of the Degradation and Production of IP_3 on Ca^{2+} Oscillations

Based on the ODE45 solver of MATLAB, we regard all formulas as a system to program and solve. Therefore, the results shown below involve all the formulas. Except for the parameter values listed in the caption of each figure, all the other parameter values and meanings are in Table 1.

What we study is biological signals. Due to the compensatory effect of biological systems, there are a few signals with stable periodic oscillations. After a period of time, the oscillation signals often return to the original equilibrium value, or reach a new equilibrium value. Numerical oscillation analysis diagrams imitate the bifurcation diagram of the dynamic system, to analyze the conditions that can produce periodic oscillation solutions for a certain length of time (1000 s in our calculation). We make numerical oscillation analysis diagrams by finding the maximum and minimum values of Ca^{2+} concentration at different k_{deg}, V_{PLC}, and IP_3 values in the last 100 s (900–1000 s). If the maximum value and minimum value are not the same, it indicates that the Ca^{2+} concentration is in the state of oscillation, and numerical oscillation analysis diagrams show that one k_{deg} or V_{PLC} value corresponds to two Ca^{2+} concentrations. If the maximum value and minimum value are the same, it indicates that the Ca^{2+} concentration is in equilibrium state, and numerical oscillation analysis diagrams show that one k_{deg} or V_{PLC} value corresponds to one Ca^{2+} concentration.

The numerical oscillation analysis diagrams show the effect of Mt and μd compartments on the $[Ca^{2+}]_{Cyt}^{eff}$ oscillatory dynamics, as functions of k_{deg} and V_{PLC}, respectively (Figure 2). They also show that the Mt compartment results in a slight decrease in the predicted oscillatory amplitude, and the μd compartment leads to an obvious decrease and the emergence of an oscillatory region at high levels of k_{deg} (range 4 to 9 s^{-1}) (Figure 2a). These results are consistent with those found by Arash Moshkforoush [34], which showed that the addition of the μd compartment resulted in the appearance of the low-energy IP_3 oscillations region in numerical oscillation analysis diagrams. k_{deg} is positively correlated with IP_3 degradation rate, and high levels of k_{deg} mean that IP_3 degrades fast; therefore, IP_3 should be kept at low levels. The Mt compartment and μd compartment can cause a decrease in the oscillatory amplitude (Figure 2b). Without μd, $[Ca^{2+}]_{Cyt}^{eff}$ oscillations appear

when V_{PLC} is in the range of 0~0.004 μMs^{-1}. While with μd, $[Ca^{2+}]^{eff}_{Cyt}$ oscillations appear when V_{PLC} is in the range of 0 to 0.003 μMs^{-1}. Figure 2a or Figure 2b shows there are little differences between the three curves at the equilibrium of $[Ca^{2+}]^{eff}_{Cyt}$. This indicated that the Mt and μd have little effect on the intracellular equilibrium of Ca^{2+} concentration.

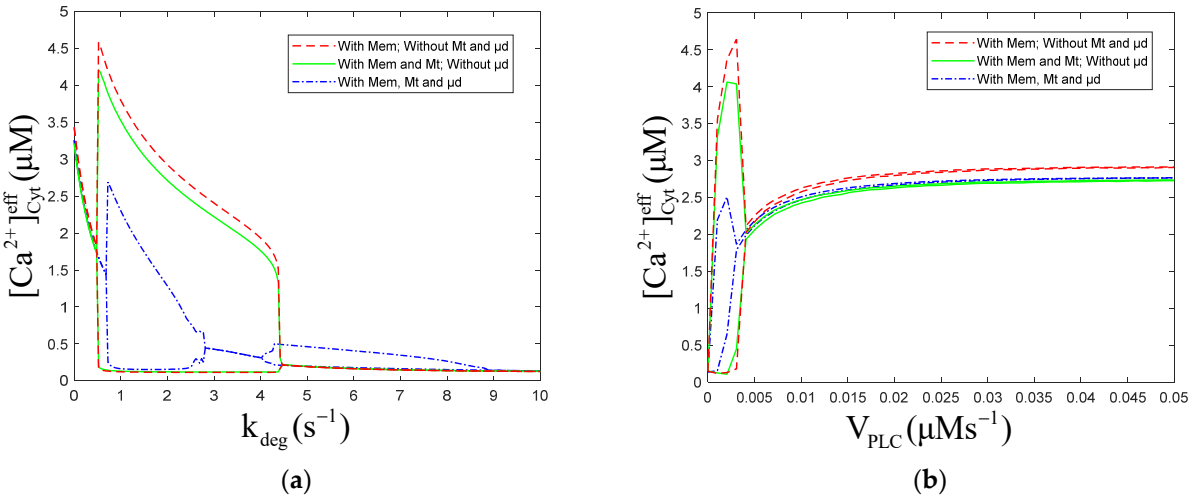

Figure 2. Numerical oscillation analysis diagrams of the $[Ca^{2+}]$ of effective cytosolic compartment ($[Ca^{2+}]^{eff}_{Cyt}$) according to (**a**) k_{deg} and (**b**) V_{PLC}. K_{PLC}= 0.12 μM, K_{deg}= 0.1 μM, D= 40 nm, and (**a**) V_{PLC} = 1 μM s^{-1}, (**b**) k_{deg}= 0.1 s^{-1}. Stimulation applied at 50 s. The other parameters and constants are taken from Table 1. V_{PLC} is the maximal production rate of PLC isoforms, K_{PLC} is the sensitivity of PLC to Ca^{2+}, k_{deg} represents the phosphorylation rate constants, K_{deg} is the half-saturation constant of IP_3 kinases. (**a**) With Mem, without Mt and μd, the oscillation range of k_{deg} is 0.48 to 4.45 s^{-1}. With Mem and Mt, without μd, the oscillation range of k_{deg} is 0.48 to 4.45 s^{-1}. With Mem, Mt and μd, the oscillation range of k_{deg} is 0.64 to 2.85 s^{-1} and 4.01 to 8.93 s^{-1}. (**b**) With Mem, without Mt and μd, the oscillation range of V_{PLC} is 0 to 0.004 s^{-1}. With Mem and Mt, without μd, the oscillation range of V_{PLC} is 0 to 0.004 s^{-1}.With Mem, Mt and μd, the oscillation range of V_{PLC} is 0 to 0.003 μM s^{-1}. From (**a**,**b**), Mem, Mt and μd all can inhibit the amplitude of calcium oscillations, but only μd can reduce oscillation range.

Consider the numerical oscillation analysis diagrams in Figure 2a, which show that with Mem, Mt, and μd, the oscillation range of k_{deg} is 0.64 to 2.85 s^{-1} and 4.01 to 8.93 s^{-1}. Therefore, four values of k_{deg} (0.1, 0.5, 1.5, and 5.0 s^{-1}) are chosen to simulate the temporal traces of $[Ca^{2+}]^{eff}_{Cyt}$. According to Figure 3a,b, $[Ca^{2+}]^{eff}_{Cyt}$ rises first, due to the stimulation, then fluctuates for a period of time and returns to the equilibrium resting state, when k_{deg} is 0.1 s^{-1} and 0.5 s^{-1},which are both out of the oscillation range. While, when k_{deg} is 1.5 s^{-1} or 5.0 s^{-1}, which both are in the oscillation range, $[Ca^{2+}]^{eff}_{Cyt}$ will maintain steady oscillations after stimulation, as shown in Figure 3c,d. The amplitude of oscillations is higher (~2 μM) and the frequency is lower (~2 oscillations/min) at lower levels of k_{deg} (Figure 3c, 1.5 s^{-1}), compared to those at higher levels of k_{deg} (amplitudes: ~0.2 μM, frequencies: ~4 oscillations/min, Figure 3d, 5.0 s^{-1}).

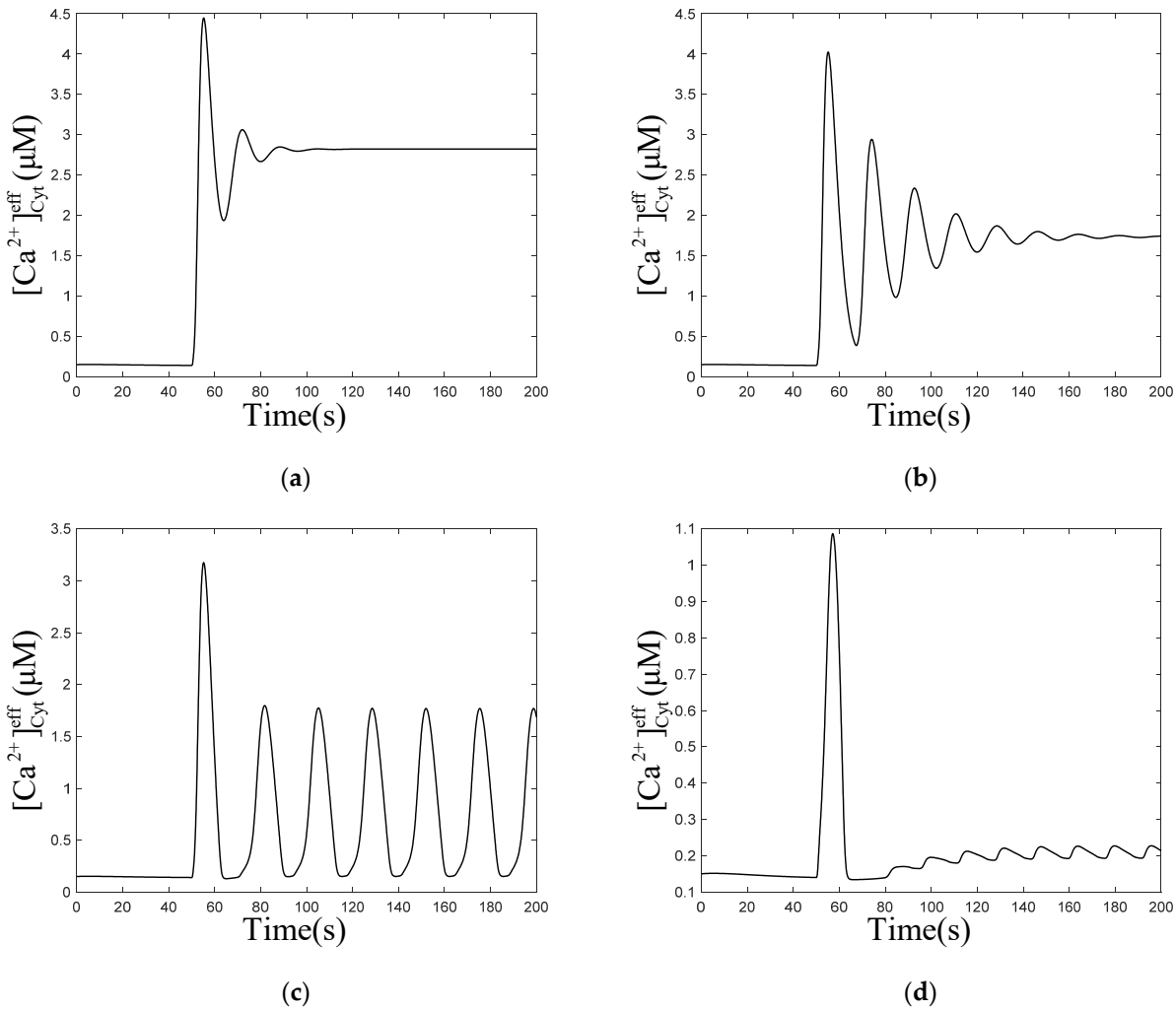

Figure 3. Numerical simulation of the $[Ca^{2+}]$ of effective cytosolic compartment ($[Ca^{2+}]^{eff}_{Cyt}$) oscillations with Mt and μd at the following different values of k_{deg}: (**a**) 0.1 s^{-1}, (**b**) 0.5 s^{-1}, (**c**) 1.5 s^{-1}, (**d**) 5.0 s^{-1}, and $V_{PLC} = 1$ μM s^{-1}, K_{PLC}= 0.12 μM, K_{deg}= 0.1 μM, D= 40 nm. Stimulation applied at 50 s. The other parameters and constants are taken from Table 1. (**a**,**b**) show that after being stimulated, the oscillations restore equilibrium in a very short time. (**c**,**d**) show that after being stimulated, the oscillations can be maintained for a long time.

When V_{PLC} is 0.001 and 0.003 μM s^{-1}, $[Ca^{2+}]^{eff}_{Cyt}$ does not rise immediately, but fluctuates to a value and forms oscillations subsequently. However, the calcium oscillations in Figure 4b are not stable, they return to an equilibrium state over time. In Figure 4c,d, Ca^{2+} concentrations only oscillate for a short period of time, to return to equilibrium. Comparing the four graphs (Figure 4a–d) shows that, with the increase in V_{PLC}, the time required for forming oscillations becomes shorter and shorter until it disappears, the frequency of oscillations decreases, but the amplitude and final equilibrium value increase. When V_{PLC} increases to a certain value, the oscillations disappear. This means that V_{PLC} affects the process of calcium oscillations from one equilibrium state to another equilibrium state. These results are consistent with most of the biological signals. Similar to the neural electrical signal, after a period of time, the oscillation signals often return to the original equilibrium value or reach a new equilibrium value.

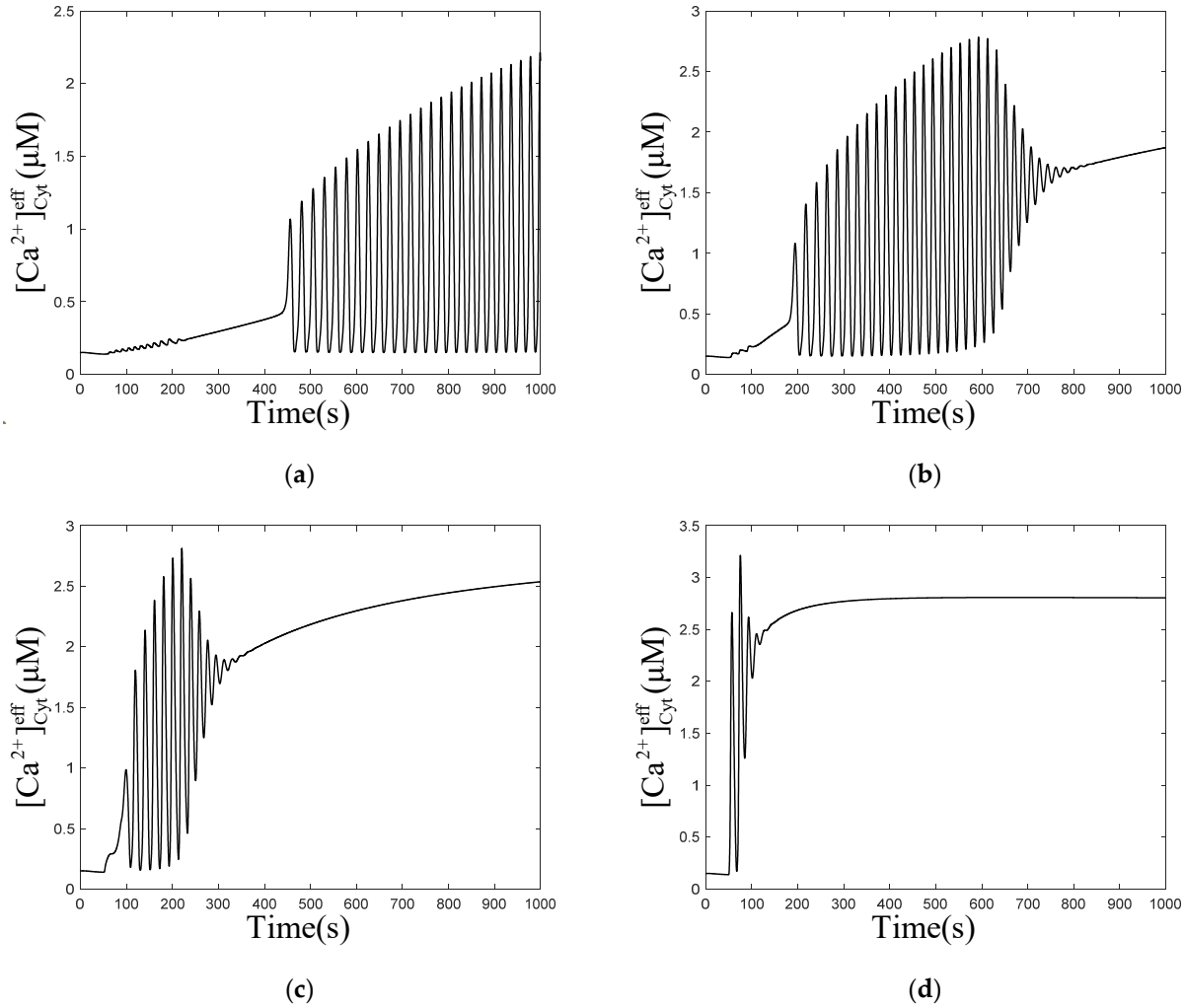

Figure 4. Numerical simulation of the $[Ca^{2+}]$ of effective cytosolic compartment ($[Ca^{2+}]^{eff}_{Cyt}$) oscillations with Mt and μd at the following different values of V_{PLC}: (**a**) 0.001 μM s^{-1}, (**b**) 0.003 μM s^{-1}, (**c**) 0.01 μM s^{-1}, (**d**) 0.1 μM s^{-1}, and k_{deg}= 0.1 s^{-1}, K_{PLC}= 0.12 μM, K_{deg}= 0.1 μM, D= 40 nm. Stimulation applied at 50 s. The other parameters and constants are taken from Table 1. (**b**–**d**) show that Ca^{2+} concentration oscillates from one equilibrium state to another equilibrium state after stimulation.

The temporal profiles of $[Ca^{2+}]$ in the following cellular compartments: Cyt, ER, Mt, μd, after stimulation, are shown in Figure 5a. When $[Ca^{2+}]_{ER}$ is at the valley value (163 μM), $[Ca^{2+}]$ in other cellular compartments are at peak value, as shown in Figure 5a. This indicates that the main Ca^{2+} filling of the Mt and μd come from the ER. The numerical simulation results also prove that high $[Ca^{2+}]_{Mt}$ is observed when global $[Ca^{2+}]_{Cyt}$ is lower, and $[Ca^{2+}]_{\mu d}$ is 20 times that of $[Ca^{2+}]_{Cyt}$, when Ca^{2+} outflows from the ER. The peak value of $[Ca^{2+}]_{\mu d}$ (37.3 μM) appears slightly earlier than those of $[Ca^{2+}]_{Cyt}$ (1.6 μM) and $[Ca^{2+}]_{Mt}$ (3.5 μM), shown in Figure 5a. This indicates that Ca^{2+} oscillations in μd are not completely synchronized with those in Cyt and Mt. The temporal profiles of $[IP_3]_{Cyt}$ and $[IP_3]_{\mu d}$ are shown in Figure 5b. After stimulation, $[IP_3]_{\mu d}$ decrease appears about 10 s earlier than that of $[IP_3]_{Cyt}$, which is in accordance with the fact that the $[Ca^{2+}]_{\mu d}$ increase happens earlier than the $[Ca^{2+}]_{Cyt}$ increase, shown in Figure 5a. The valley value of $[IP_3]_{Cyt}$ (0.56 μM) is lower than that of $[IP_3]_{\mu d}$ (0.61 μM) in Figure 5b.

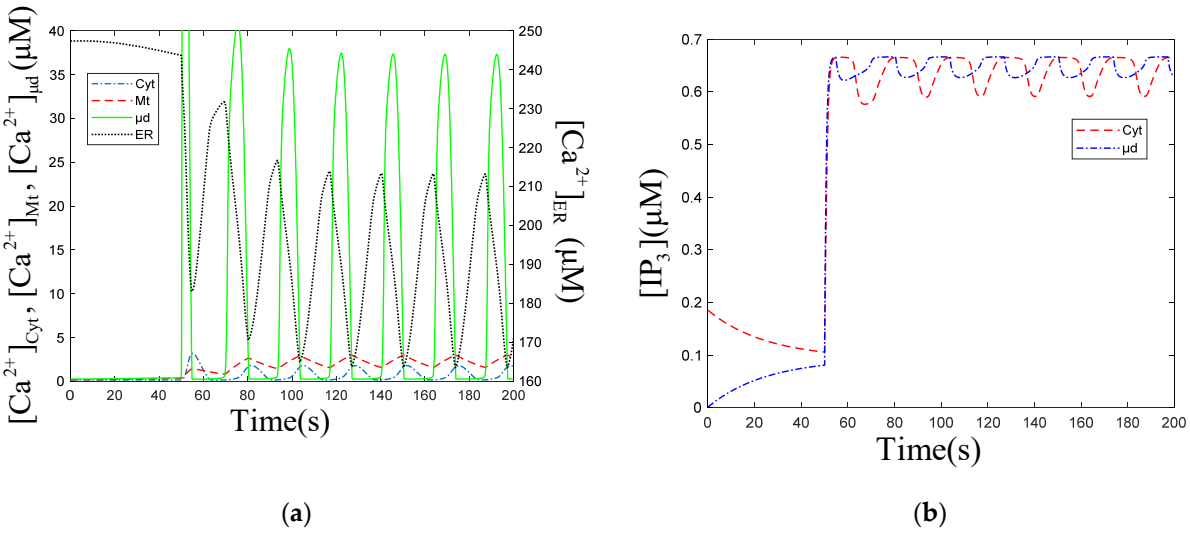

(**a**) (**b**)

Figure 5. (**a**) Ca^{2+} oscillations profiles in each cellular compartment. $[Ca^{2+}]_{ER}$, $[Ca^{2+}]_{Cyt}$, $[Ca^{2+}]_{Mt}$ and $[Ca^{2+}]_{\mu d}$ mean Ca^{2+} concentration of ER, Cyt, Mt and μd. (**b**) IP_3 oscillations in Cyt and μd. $[IP_3]_{\mu d}$ means IP_3 concentration of μd. $V_{PLC} = 1$ μM s^{-1}, $k_{deg} = 1.5$ s^{-1}, $K_{PLC} = 0.12$ μM, $K_{deg} = 0.1$ μM, $D = 40$ nm. Stimulation applied at 50 s. The other parameters and constants are taken from Table 1. (**a**) The amplitude of $[Ca^{2+}]_{ER}$ oscillations is 47.86 μM, the frequency is 22.4 s. The amplitude of $[Ca^{2+}]_{Cyt}$ oscillations is 1.76 μM, the frequency is 23.4 s. The amplitude of $[Ca^{2+}]_{Mt}$ oscillations is 2.94 μM, the frequency is 23.3 s. The amplitude of $[Ca^{2+}]_{\mu d}$ oscillations is 37.32 μM, the frequency is 23.7 s. (**b**) The amplitude of $[IP_3]_{Cyt}$ oscillations is 0.07 μM, the frequency is 23.2 s. The amplitude of $[IP_3]_{\mu d}$ oscillations is 0.04 μM, the frequency is 23.8 s. (**a**,**b**) show that the oscillations are out of sync, but the frequencies are pretty much the same.

3.2. Effect of the ER–Mt Distance (D) on Ca^{2+} Oscillations

Figure 6a,c show that with the increase in the ER–Mt distance, the amplitude of $[Ca^{2+}]_{Cyt}$ oscillations increased slightly. The numerical simulation results of Qi [33] show that with increasing ER–Mt distance at $D < 20$ nm, the $[Ca^{2+}]_{Cyt}$ amplitudes decrease, while at $D > 20$ nm, the $[Ca^{2+}]_{Cyt}$ amplitudes increase. A result similar to Qi appears in our model, at $D = 40$ nm, the $[Ca^{2+}]_{\mu d}$ amplitude is the highest in Figure 6b. Moreover, Figure 6d shows that with ER–Mt distance increases at $D < 65$ nm, the $[Ca^{2+}]_{\mu d}$ amplitudes increase, while at $D > 65$ nm, the $[Ca^{2+}]_{\mu d}$ amplitudes decrease with ER–Mt distance increases. In Figure 6f, there is also an obvious inflection point of $[Ca^{2+}]^{eff}_{Cyt}$ amplitudes at $D = 65$ nm. When $D > 65$ nm, the $[Ca^{2+}]^{eff}_{Cyt}$ amplitudes increase faster than $D < 65$ nm, of which the amplitudes maintain around 1.6 μM. Combining Figure 6d,f, we find that in this model, when D is larger than 65 nm, the influence of μd on $[Ca^{2+}]^{eff}_{Cyt}$ oscillations is weak. This is a mathematical explanation of why the μd functional region should have a small distance. Figure 6e shows that $[Ca^{2+}]_{ER}$ amplitudes increase with ER–Mt distance increases, meaning the ER releases more Ca^{2+} under larger ER–Mt distances. This explains why the amplitude of $[Ca^{2+}]_{Cyt}$ and $[Ca^{2+}]^{eff}_{Cyt}$ oscillations increase with ER–Mt distance increases.

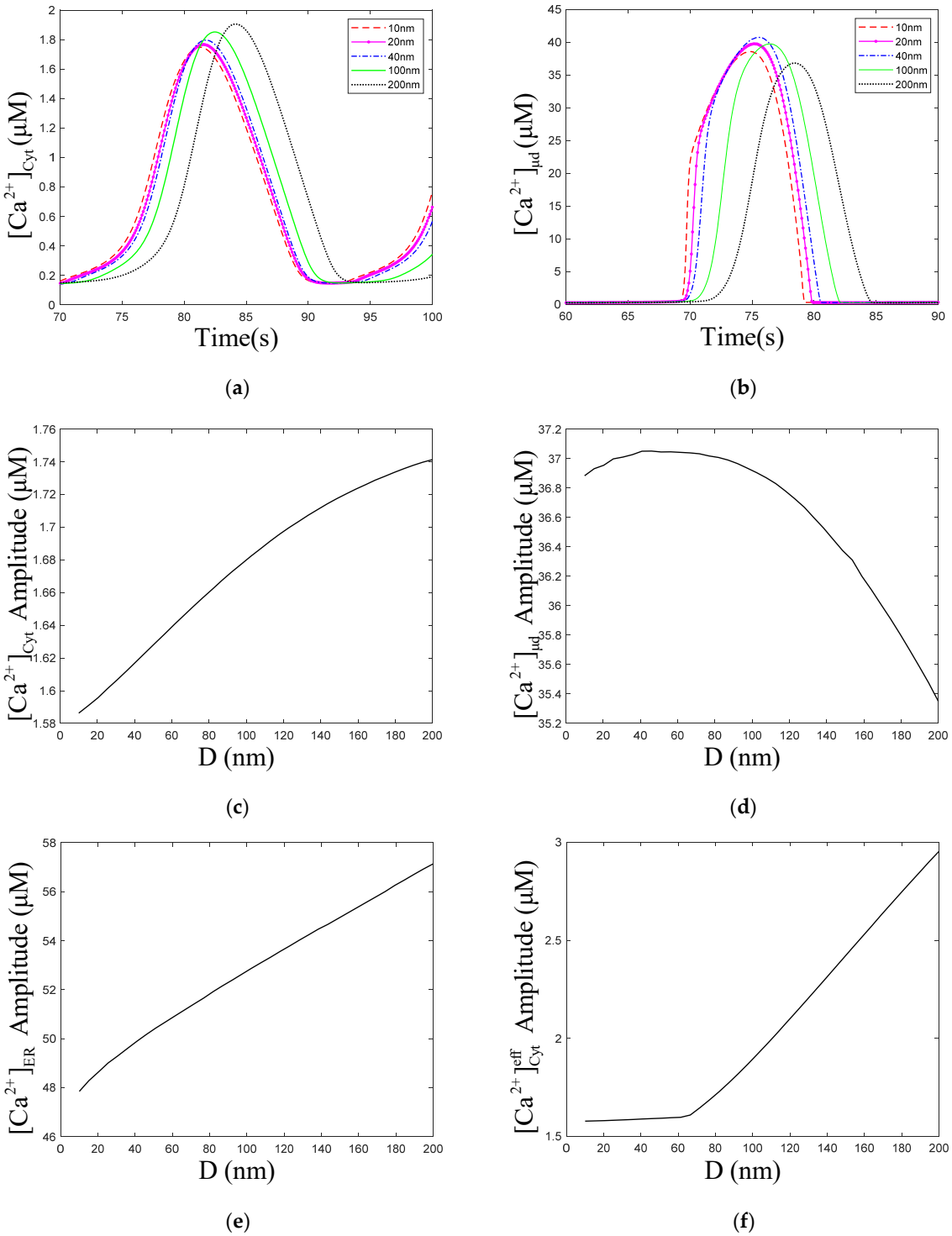

Figure 6. Dynamics modulated by the ER–Mt distance (D). $V_{PLC} = 1$ μM s^{-1}, k_{deg}= 1.5 s^{-1}, K_{PLC}= 0.12 μM, K_{deg}= 0.1 μM. Stimulation applied at 50 s. The other parameters and constants are taken from Table 1. (**a**) Ca^{2+} concentration of Cyt ($[Ca^{2+}]_{Cyt}$) oscillations as a function of time at the following different Ds: D = 10, 20, 40, 100 and 200 nm. (**b**) Ca^{2+} concentration of μd ($[Ca^{2+}]_{\mu d}$) oscillations as a function of time at the following different Ds: D = 10, 20, 40, 100 and 200 nm. (**c**) The amplitudes of Ca^{2+} concentration of Cyt ($[Ca^{2+}]_{Cyt}$) oscillations as a function of D. (**d**) The amplitudes of Ca^{2+} concentration of μd ($[Ca^{2+}]_{\mu d}$) as a function of D. (**e**) The amplitudes of Ca^{2+} concentration of ER $[Ca^{2+}]_{ER}$ as a function of D. (**f**) The amplitudes of Ca^{2+} concentration of effective cytosolic compartment ($[Ca^{2+}]^{eff}_{Cyt}$) as a function of D. With the increase in the ER–Mt distance, (**a**) the amplitude of $[Ca^{2+}]_{Cyt}$ oscillations increases, (**b**) the amplitude of $[Ca^{2+}]_{\mu d}$ oscillations decreases. (**d**,**f**) show that the effect of D in calcium oscillations is weak when D is great than 65 nm.

Figure 7 shows that the period of $[Ca^{2+}]_{Cyt}$ and $[Ca^{2+}]_{\mu d}$ oscillations increases with ER–Mt distance increases. In combination with Figure 5a, we find that $[Ca^{2+}]_{\mu d}$ is higher than $[Ca^{2+}]_{Cyt}$ and their oscillations are not synchronous, but the periods as well as the frequency of oscillations are the same. When D = 10, 200 nm, the period of $[Ca^{2+}]_{Cyt}$ and $[Ca^{2+}]_{\mu d}$ is 23.2 and 23.3 s, and 25.5 and 25.5 s, respectively. Figure 7 shows that the period and distance have an approximate linear relationship; therefore, we can obtain the slopes of $[Ca^{2+}]_{Cyt}$ (0.01244) and $[Ca^{2+}]_{\mu d}$ (0.01232) by fitting. From a mathematical point, this result is beyond our expectation, because in this model, Cyt and μd are calculated as two rooms, and there is only a diffusion relationship between the two rooms. While from a cellular physiological point, this result is reasonable. In the model, the μd is a region that we hypothesize from the cytoplasm. However, in the actual cell, it is a part of the Cyt, hence both the frequencies should be the same. Meanwhile, the frequency of calcium oscillations is one of the ways that cellular calcium signaling transmits information. When the whole intracellular calcium signaling is formed, the same frequency can transmit the same information. Therefore, the calcium signaling must be consistent to prevent cells from receiving different information at the same time, causing functional disorders.

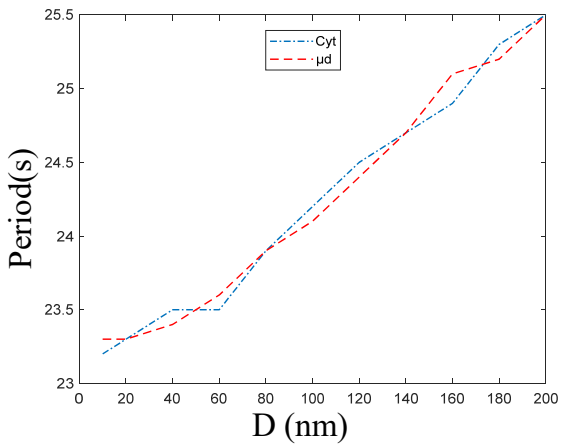

Figure 7. The period of Ca^{2+} concentration of Cyt and μd oscillations at the following different ER–Mt distances (D): 10, 20, 40 60, 80, 100, 120, 140, 160, 180, 200 nm. V_{PLC} = 1 μM s^{-1}, k_{deg}= 1.5 s^{-1}, K_{PLC}= 0.12 μM, K_{deg}= 0.1 μM. The other parameters and constants are taken from Table 1. These two curves fit well, meaning that calcium oscillations of Cyt and μd have same frequency under different ER–Mt distances.

3.3. *Effect of the $[IP_3]_{Cyt}$ on Ca^{2+} Oscillations*

The numerical oscillation analysis diagrams in Figure 8a show that the Mt, μd, and Mem compartments can each reduce the amplitude of $[Ca^{2+}]^{eff}_{Cyt}$ oscillations. Contrasting the dot curve with the solid curve, we can find that the addition of the μd compartment causes $[Ca^{2+}]^{eff}_{Cyt}$ oscillation regions at low-level $[IP_3]_{Cyt}$ of 0.08~0.27 μM. Comparing the dot curve and dot solid curve, we find that the Mem compartment makes the $[Ca^{2+}]^{eff}_{Cyt}$ oscillations at low-level $[IP_3]_{Cyt}$ disappear. The Mt compartment has a slight effect on the left and right bifurcation point value of $[Ca^{2+}]^{eff}_{Cyt}$ oscillations. The $[Ca^{2+}]^{eff}_{Cyt}$ oscillations region of the model, with Mt, μd, and Mem, shrink obviously, meaning that the μd and Mem compartments limit the range of $[Ca^{2+}]^{eff}_{Cyt}$ oscillations. From Figure 8a, we can also draw a similar conclusion as Figure 2, which is that the presence or absence of Mt, μd, and Mem have little effect on the equilibrium calcium concentration.

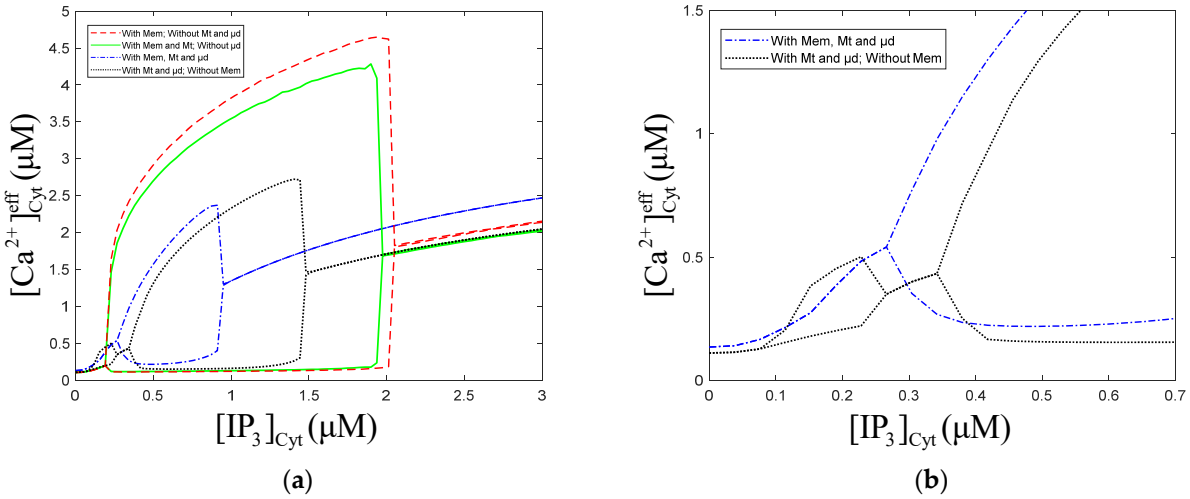

Figure 8. Numerical oscillation analysis diagrams with/without the Mt, μd and Mem. $V_{PLC} = 1$ μM s^{-1}, k_{deg}= 1.5 s^{-1}, K_{PLC}= 0.12 μM, K_{deg}= 0.1 μM. Stimulation applied at 50 s. The other parameters and constants are taken from Table 1. (**b**) is a larger view of $[IP_3]_{Cyt}$ from 0 to 0.6 μM in figure (**a**) of with/without Mem. $[IP_3]_{Cyt}$ means IP_3 concentration of Cyt. $[Ca^{2+}]^{eff}_{Cyt}$ means Ca^{2+} concentration of effective cytosolic compartment. (**a**) With Mt and μd, without Mem, the oscillation range of $[IP_3]_{Cyt}$ is 0.07 to 0.26 μM and 0.34 to 1.51 μM. With Mt, μd, and Mem, the oscillation range of $[IP_3]_{Cyt}$ is 0.26 to 0.94 μM. (**b**) Mem limits the calcium oscillations range of low IP_3 concentration.

4. Discussion and Conclusions

In Qi's model [33], the IP_3R–MCU distance is regarded as the main factor by which μd affects calcium oscillations. He links the ER with Mt by one-dimensional diffusion of Ca^{2+} between IP_3R and MCU. However, with the distance increases, the influence of Ca^{2+} diffusion in other directions will be more significant. Hence, the one-dimensional diffusion assumption will make the calculation error of $[Ca^{2+}]_{\mu d}$ larger, and the error of calcium oscillations larger. Therefore, in our model, we assume that the μd is a separate chamber with volume. As shown in Figure 6d, $[Ca^{2+}]_{\mu d}$ increases a little before 65 nm and decrease subsequently. From Figure 6e, we find that the ER–Mt distance increase makes the ER release more Ca^{2+}. This is because IP_3R has a Ca^{2+} inhibition binding site, so when Ca^{2+} binds to this site, IP_3 activity is inhibited. As the ER–Mt distance increases, Ca^{2+} can spread faster; therefore, the probability of Ca^{2+} binding to the inhibition site decreases, so Ca^{2+} released by IP_3 increases. Hence, there is a little upward trend of $[Ca^{2+}]_{\mu d}$, and, later, the effect of the increased volume of μd is greater than the release of Ca^{2+}, and $[Ca^{2+}]_{\mu d}$ begins to decrease. However, in Qi's result, $[Ca^{2+}]_{\mu d}$ was decreasing all the time. Arash Moshkforoush's model [34] does not consider the degradation and production of IP_3; therefore, the concentration of IP_3 in the cells is constant, which is not a physiological reality. IP_3 dynamic behaviors have a significant effect on the range of parameter values and the oscillation patterns of $[Ca^{2+}]_{Cyt}$ oscillations [43]. Inhibition of protein kinase C eliminates Ca^{2+} oscillations, while IP_3 formation is still maintained [44]. This is also shown in Figure 2a,b, which shows that at different degradation and production levels of IP_3, there are different amplitudes and frequencies of $[Ca^{2+}]_{Cyt}$ oscillations.

In this paper, the dynamic model of calcium oscillations in MCs is developed, which considers the major cellular compartments (Cyt, Mem, ER, and Mt), Ca^{2+} channels and buffer in these compartments, and the μd composed of the ER and Mt. In our simulations, the Mt and μd compartments can reduce the amplitude of $[Ca^{2+}]^{eff}_{Cyt}$ oscillations. With the addition of the μd compartment, an oscillatory region will appear at high levels of k_{deg} (4 to 9 s^{-1}) and at low levels of $[IP_3]_{Cyt}$ (0.08~0.27 μM), shown in Figures 2a and 8a. Our model also shows that different concentrations of IP_3 stimulation will change the amplitude

and frequency of $[Ca^{2+}]_{Cyt}$ oscillations. The amplitude of $[Ca^{2+}]^{eff}_{Cyt}$ oscillations increases, and the frequency of $[Ca^{2+}]^{eff}_{Cyt}$ oscillations decreases with $[IP_3]_{Cyt}$ increases. Figure 4b shows that the $[Ca^{2+}]^{eff}_{Cyt}$ oscillations process is in line with the actual law of cell calcium signal generation. The calcium signal can be divided into the following three levels: (i) at first, being the most fundamental event, a very low level of stimulation will cause a brief opening of a single channel and the release of calcium, which is called calcium blips; (ii) then, there is the basic event, which results from a small group of channels opening and the release of calcium, to form calcium sparks; (iii) finally, the synchronization of a large number of fundamental events produces the global calcium signal, and subsequently restores the resting state. According to our results, the amplitude of $[Ca^{2+}]_{Cyt}$ oscillations increases with the increase in the ER–Mt distance. Moreover, the $[Ca^{2+}]_{\mu d}$ amplitude also increases with the increase in the ER–Mt distance at $D < 65$ nm, but decreases with the increase in the ER–Mt distance at $D > 65$ nm. Therefore, we believe that μd has a better regulation effect on $[Ca^{2+}]_{Cyt}$ oscillations when the ER–Mt distance is less than about 65 nm, which also provides reference for determining the distance of μd in the subsequent studies. The periods of $[Ca^{2+}]_{Cyt}$ and $[Ca^{2+}]_{\mu d}$ oscillations are the same at different ER–Mt distances, and they increase with the ER–Mt distance. Meanwhile, from Figures 5a and 7, we can understand that $[Ca^{2+}]_{\mu d}$ is 20 times higher than $[Ca^{2+}]_{Cyt}$, and their oscillations are not synchronous. The presence of μd causes the ER to release less Ca^{2+}, and the effect of μd decreases with ER–Mt distance increases. This proves that μd acts as a buffer against the release of Ca^{2+} from the ER. All these results suggest that μd plays an important role in controlling $[Ca^{2+}]_{Cyt}$ oscillations at $D < 65$ nm. The degradation and production of IP_3 can also regulate $[Ca^{2+}]_{Cyt}$ oscillations by maintaining different levels of $[IP_3]_{Cyt}$. As shown in Figure 5b, before stimulation, $[IP_3]_{Cyt}$ and $[IP_3]_{\mu d}$ get closer, due to the diffusion between Cyt and μd. This is because the IP_3 production and degradation of μd and Cyt maintain dynamic equilibrium at the initial moment, but the concentration of IP_3 will affect $[Ca^{2+}]_{Cyt}$ oscillations; therefore, we assume that the production and degradation of IP_3 are both zero before the stimulation (50 s), to reduce the impact of IP_3 on calcium oscillations in the study of V_{PLC} and k_{deg}. Then, at this time, the dynamic equilibrium is destroyed, and the concentrations of μd and Cyt are close to each other. We already know that the concentration of IP_3 also has an effect on oscillations, hence the given concentration of IP_3 is not used as the stimulation, but the system is deviated from the equilibrium state through diffusion after the production and degradation of IP_3 is assumed to be zero, and then the values of V_{PLC} and k_{deg} are restored, so as to reduce the impact of IP_3 on calcium oscillations in the study of V_{PLC} and k_{deg}.

From the biological point of view, due to the compensatory effect of biological systems, there are a few signals with stable periodic oscillations. After a period of time, the oscillation signals often return to the original equilibrium value, or reach a new equilibrium value. This is consistent with Figure 4b–d. IP_3R is regulated by Ca^{2+} in a biphasic manner; therefore, IP_3R activity is inhibited at higher Ca^{2+} concentrations. When the ER–Mt distance increases in our model, the volume of μd increases and the Ca^{2+} concentration of μd gradually decreases, and this causes the activity of IP_3R to increase; therefore, more Ca^{2+} will outflow from the ER through the IP_3R channels, causing the ER calcium oscillations amplitude increases shown in Figure 6e, and the cytoplasmic Ca^{2+} concentration increases shown in Figure 6c. Calcium oscillations have been widely accepted as a universal signal mode in cells. With the in-depth study of calcium oscillations, the basic theory of calcium oscillations regulating downstream biological effects through its frequency has been established [45,46]. In Figure 7, the calcium oscillation frequencies of Cyt and μd calculated by our model are basically the same, which also implies that the frequency of calcium oscillations is one of the ways of signal transmission.

In summary, the study provides a dynamic model that simulates calcium oscillations in mast cells and provides a theoretical basis for the mast cell calcium signal observed in the

experiment. This enabled us to consolidate previous theoretical and experimental findings. The model results showed that Mem, Mt, and μd can all reduce the amplitude of $[Ca^{2+}]_{Cyt}$ oscillations. Moreover, μd can play a critical role in Ca^{2+} dynamics at appropriate ER–Mt distances (less than 65 nm). In future work, we will continue to study the influence of mitochondrial ATP and important calcium channel parameters on $[Ca^{2+}]_{Cyt}$ oscillations. Additionally, we will improve our model by adding other intracellular calcium pools (such as nucleus, Golgi apparatus, etc.), to make our model more accurate. Although we have oversimplified some details, we believe that this model is still useful and can provide us with some insights into the mechanism of mast cell calcium signaling regulation.

Author Contributions: Conceptualization, W.Y.; software, M.S.; formal analysis, M.S., Y.L.; data curation, M.S.; writing—original draft preparation, M.S.; writing—review and editing, W.Y., Y.L.; visualization, M.S., Y.L., W.Y.; supervision, W.Y.; project administration, W.Y.; funding acquisition, W.Y. All authors have read and agreed to the published version of the manuscript.

Funding: This research was funded by National Natural Science Foundation of China (grant number: 12172092, 82174488) and Shanghai Key Laboratory of Acupuncture Mechanism and Acupoint Function (grant number: 21DZ2271800).

Institutional Review Board Statement: Not applicable.

Informed Consent Statement: Not applicable.

Data Availability Statement: Not applicable.

Conflicts of Interest: The authors declare no conflict of interest.

References

1. Ding, N.; Jiang, J.; Qin, P.; Wang, Q.; Hu, J.; Li, Z. Mast cells are important regulator of acupoint sensitization via the secretion of tryptase, 5-hydroxytryptamine, and histamine. *PLoS ONE* **2018**, *13*, e0194022. [CrossRef] [PubMed]
2. Berridge, M.J.; Bootman, M.D.; Roderick, H.L. Calcium signalling: Dynamics, homeostasis and remodelling. *Nat. Rev. Mol. Cell Biol.* **2003**, *4*, 517–529. [CrossRef]
3. Parekh, A.B. Decoding cytosolic Ca^{2+} oscillations. *Trends Biochem. Sci.* **2011**, *36*, 78–87. [CrossRef]
4. Zhu, L.; Luo, Y.; Chen, T.; Chen, F.; Wang, T.; Hu, Q. Ca^{2+} oscillation frequency regulates agonist-stimulated gene expression in vascular endothelial cells. *J. Cell Sci.* **2008**, *121*, 2511–2518. [CrossRef]
5. Smedler, E.; Uhlén, P. Frequency decoding of calcium oscillations. *Biochim. Biophys. Acta* **2013**, *1840*, 964–969. [CrossRef]
6. Capite, J.D.; Parekh, A.B. CRAC channels and Ca^{2+} signaling in mast cells. *Immunol. Rev.* **2010**, *231*, 45–58. [CrossRef]
7. Hoth, M.; Penner, R. Depletion of intracellular calcium stores activates a calcium current in mast cells. *Nature* **1992**, *355*, 353–356. [CrossRef]
8. Baker, H.L.; Errington, R.J.; Davies, S.C.; Campbell, A.K. A mathematical model predicts that calreticulin interacts with the endoplasmic recticulum Ca. *Biophys. J.* **2002**, *82*, 582–590. [CrossRef]
9. Contreras, L.; Drago, I.; Zampese, E.; Pozzan, T. Mitochondria: The calcium connection. *BBA Bioenerg.* **2010**, *1797*, 607–618. [CrossRef] [PubMed]
10. Hajno'czky, G.; Robb-Gaspers, L.D.; Seitz, M.B.; Thomas, A.P. Decoding of cytosolic calcium oscillations in the mitochondria. *Cell* **1995**, *82*, 415–424. [CrossRef]
11. Samanta, K.; Douglas, S.; Parekh, A.B. Mitochondrial Calcium Uniporter MCU Supports Cytoplasmic Ca^{2+} Oscillations, Store-Operated Ca^{2+} Entry and Ca^{2+}-Dependent Gene Expression in Response to Receptor Stimulation. *PLoS ONE* **2014**, *9*, e101188. [CrossRef] [PubMed]
12. Ishii, K.; Hirose, K.; Iino, M. Ca^{2+} shuttling between endoplasmic reticulum and mitochondria underlying Ca^{2+} oscillations. *EMBO J.* **2006**, *7*, 390–396. [CrossRef]
13. Rizzuto, R.; De Stefani, D.; Raffaello, A.; Mammucari, C. Mitochondria as sensors and regulators of calcium signalling. *Nat. Rev. Mol. Cell Biol.* **2012**, *13*, 566–578. [CrossRef] [PubMed]
14. De Stefani, D.; Rizzuto, R.; Pozzan, T. Calcium in Mitochondria Back and Forth. *Annu. Rev. Biochem.* **2016**, *85*, 161–192. [CrossRef] [PubMed]
15. Csordás, G.; Renken, C.; Várnai, P.; Walter, L.; Weaver, D.; Buttle, K.F.; Balla, T.; Mannella, C.A.; Hajnóczky, G. Structural and functional features and significance of the physical linkage between ER and mitochondria. *J. Cell Biol.* **2006**, *174*, 915–921. [CrossRef]
16. Raturi, A.; Simmen, T. Where the endoplasmic reticulum and the mitochondrion tie the knot: The mitochondria-associated membrane (MAM). *Biochim. Biophys. Acta* **2013**, *1833*, 213–224. [CrossRef]

17. Patergnani, S.; Suski, J.M.; Agnoletto, C.; Bononi, A.; Bonora, M.; De Marchi, E.; Giorgi, C.; Marchi, S.; Missiroli, S.; Poletti, F.; et al. Calcium signaling around Mitochondria Associated Membranes (MAMs). *Cell Commun. Signal.* **2011**, *9*, 19. [CrossRef]
18. de Brito, O.M.; Scorrano, L. An intimate liaison: Spatial organization of the endoplasmic reticulum–mitochondria relationship. *EMBO J.* **2010**, *29*, 2715–2723. [CrossRef] [PubMed]
19. Wei, Y.; Huang, H.; Ding, G. A dynamic model of calcium signaling in mast cells and LTC4 release induced by mechanical stimuli. *Chin. Sci. Bull.* **2014**, *59*, 956–963.
20. Miyakawa, T.; Mizushima, A.; Hirose, K.; Yamazawa, T.; Bezprozvanny, I.; Kurosaki, T.; Iino, M. Ca^{2+}-sensor region of IP_3 receptor controls intracellular Ca^{2+} signaling. *EMBO J.* **2001**, *20*, 1674–1680. [CrossRef]
21. Berridge, M.J. Inositol trisphosphate and calcium signalling mechanisms. *Biochim. Biophys. Acta* **2009**, *1793*, 933–940. [CrossRef]
22. Bezprozvanny, I.; Watras, J.; Ehrlich, B.E. Bell-shaped calcium-response curves of Ins (1,4,5) P3- and calcium-gated channels from endoplasmic reticulum of cerebellum. *Nature* **1991**, *351*, 751–754. [CrossRef]
23. Csordás, G.; Várnai, P.; Golenár, T.; Roy, S.; Purkins, G.; Schneider, T.G.; Balla, T.; Hajnóczky, G. Imaging interorganelle contacts and local calcium dynamics at the ER-mitochondrial interface. *Mol. Cell* **2010**, *39*, 121–132. [CrossRef]
24. Giacomello, M.; Drago, I.; Bortolozzi, M.; Scorzeto, M.; Gianelle, A.; Pizzo, P.; Pozzan, T. Ca^{2+} hot spots on the mitochondrial surface are generated by Ca^{2+} mobilization from stores, but not by activation of store-operated Ca^{2+} channels. *Mol. Cell* **2010**, *38*, 280–290. [CrossRef]
25. Williams, G.S.; Boyman, L.; Chikando, A.C.; Khairallah, R.J.; Lederer, W.J. Mitochondrial calcium uptake. *Proc. Natl. Acad. Sci. USA* **2013**, *110*, 10479–10486. [CrossRef]
26. Di Capite, J.; Shirley, A.; Nelson, C.; Bates, G.; Parekh, A.B. Intercellular Ca^{2+} wave propagation involving positive feedback between CRAC channels and cysteinyl leukotrienes. *FASEB J.* **2009**, *23*, 894–905. [CrossRef] [PubMed]
27. Osipchuk, Y.; Cahalan, M. Cell-to-cell spread of calcium signals mediated by ATP receptors in mast cells. *Nature* **1992**, *359*, 241–244. [CrossRef] [PubMed]
28. Dupont, G.; Berridge, M.J. Minimal model for signal-induced Ca^{2+} oscillations and for their frequency encoding through protein phosphorylation. *Proc. Natl. Acad. Sci. USA* **1990**, *87*, 1461–1465.
29. Hufer, T. Model of Intercellular Calcium Oscillations in Hepatocytes: Synchronization of Heterogeneous Cells. *Biophys. J.* **1999**, *77*, 1244–1256. [CrossRef]
30. Li, Y.X.; Rinzel, J. Equations for $InsP_3$ Receptor-mediated $[Ca^{2+}]i$ Oscillations Derived from a Detailed Kinetic Model: A Hodgkin-Huxley Like Formalism. *J. Theor. Biol.* **1994**, *166*, 461–473. [CrossRef] [PubMed]
31. Falcke, M.; Hudson, J.; Camacho, P.; Lechleiter, J. Impact of Mitochondrial Ca^{2+} Cycling on Pattern Formation and Stability. *Biophys. J.* **1999**, *77*, 37–44. [CrossRef]
32. Xiao-Min, S.; Zeng-Rong, L. An Intracellular Calcium Oscillations Model Including Mitochondrial Calcium Cycling. *Chin. Phys. Lett.* **2005**, *22*, 3206. [CrossRef]
33. Qi, H.; Li, L.; Shuai, J. Optimal microdomain crosstalk between endoplasmic reticulum and mitochondria for Ca^{2+} oscillations. *Sci. Rep.* **2015**, *5*, 7984. [CrossRef]
34. Moshkforoush, A.; Ashenagar, B.; Tsoukias, N.M.; Alevriadou, B.R. Modeling the role of endoplasmic reticulum-mitochondria microdomains in calcium dynamics. *Sci. Rep.* **2019**, *9*, 17072. [CrossRef] [PubMed]
35. Kapela, A.; Bezerianos, A.; Tsoukias, N.M. A mathematical model of Ca^{2+} dynamics in rat mesenteric smooth muscle cell: Agonist and NO stimulation. *J. Theor. Biol.* **2008**, *253*, 238–260. [CrossRef] [PubMed]
36. Silva, H.S.; Kapela, A.; Tsoukias, N.M. A mathematical modelof plasma membrane electro physiology and calcium dynamics in vascular endothelial cells. *Am. J. Physiol. Cell Physiol.* **2007**, *293*, 277–293. [CrossRef] [PubMed]
37. Csordas, G.; Hajnoczky, G. Plasticity of Mitochondrial Calcium Signaling. *J. Biol. Chem.* **2003**, *278*, 42273–42282. [CrossRef] [PubMed]
38. Chalmers, S.; Mccarron, J.G. The mitochondrial membrane potential and Ca^{2+} oscillations in smooth muscle. *J. Cell Sci.* **2008**, *121 Pt 1*, 75–85. [CrossRef] [PubMed]
39. Mccarron, J.G.; Olson, M.L.; Chalmers, S. Mitochondrial regulation of cytosolic Ca^{2+} signals in smooth muscle. *Pflug. Arch.* **2012**, *464*, 51–62. [CrossRef]
40. Rizzuto, R.; Pinton, P.; Carrington, W.; Fay, F.S.; Fogarty, K.E.; Lifshitz, L.M.; Tuft, R.A.; Pozzan, T. Close contacts with the endoplasmic reticulum as determinants of mitochondrial Ca^{2+} responses. *Science* **1998**, *280*, 1763–1766. [CrossRef]
41. Giedt, R.J.; Pfeiffer, D.R.; Matzavinos, A.; Kao CYAlevriadou, B.R. Mitochondrial dynamics and motility inside living vascular endothelial cells: Role of bioenergetics. *Ann. Biomed. Eng.* **2012**, *52*, 348–356. [CrossRef]
42. Higgins, E.R.; Cannell, M.B.; Sneyd, J. A buffering SERCA pump in models of calcium dynamics. *Biophys. J.* **2006**, *91*, 151–163. [CrossRef] [PubMed]
43. Kummer, U.; Olsen, L.F.; Dixon, C.J.; Green, A.K.; Bornberg-Bauer, E.; Baier, G. Switching from simple to complex oscillations in calcium signaling. *Biphys. J.* **2000**, *79*, 1188–1195. [CrossRef]
44. Nash, M.S.; Young, K.W.; Challiss, R.A.J.; Nahorski, S.R. Intracellular signalling: Receptor-specific messenger oscillations. *Nature* **2011**, *413*, 381–382. [CrossRef] [PubMed]

45. Politi, A.; Gaspers, L.D.; Thomas, A.P.; Höfer, T. Models of IP_3 and Ca^{2+} oscillations: Frequency encoding and identification of underlying feedbacks. *Biophys. J.* **2006**, *90*, 3120–3133. [CrossRef] [PubMed]
46. Michalak, M.; Parker, J.R.; Opas, M. Ca^{2+} signaling and calcium binding chaperones of the endoplasmic reticulum. *Cell Calcium* **2002**, *32*, 269–278. [CrossRef]